Ultramicroscopy 159 (2015) 240–247

Contents lists available at ScienceDirect

Ultramicroscopy

journal homepage: www.elsevier.com/locate/ultramic

Atomic scale investigation of non-equilibrium segregation of boron in a quenched Mo-free martensitic steel

Y.J. Li *, D. Ponge *, P. Choi, D. Raabe

Max-Planck Institut für Eisenforschung, Max-Planck-Str. 1, D-40237 Düsseldorf, Germany

ARTICLE INFO

Article history:
Received 29 August 2014
Received in revised form
23 January 2015
Accepted 5 March 2015
Available online 14 March 2015

Keywords:
Atom probe tomography
Site-specific sample preparation
Martensitic steels
Boron segregation
Prior austenite grain boundaries
Non-equilibrium segregation

ABSTRACT

B-added low carbon steels exhibit excellent hardenability. The reason has been frequently attributed to B segregation at prior austenite grain boundaries, which prevents the austenite to ferrite transformation and favors the formation of martensite. The segregation behavior of B at prior austenite grain boundaries is strongly influenced by processing conditions such as austenitization temperatures and cooling rates and by alloying elements such as Mo, Cr, and Nb. Here an local electrode atom probe was employed to investigate the segregation behavior of B and other alloying elements (C, Mn, Si, and Cr) in a Cr-added Mo-free martensitic steel. Similar to our previous results on a Mo-added steel, we found that in both steels B is segregated at prior austenite grain boundaries with similar excess values, whereas B is neither detected in the martensitic matrix nor at martensite–martensite boundaries at the given cooling rate of 30 K/s. These results are in agreement with the literature reporting that Cr has the same effect on hardenability of steels as Mo in the case of high cooling rates. The absence of B at martensite–martensite boundaries suggests that B segregates to prior austenite grain boundaries via a non-equilibrium mechanism. Segregation of C at all boundaries such as prior austenite grain boundaries and martensite–martensite boundaries may occur by an equilibrium mechanism.

1. Introduction

It is well known that B plays an important role as a hardenability agent in steels [1,2]. The advantages of B over the traditional alloying elements such as Cr, Mo, Mn, V, and Ni are its lower cost and a smaller quantity required for a remarkable hardenability in low-carbon alloys. For example, an addition of 20–30 wt ppm B to low alloyed steels provides the same effect on improving hardenability as 0.4–0.7 wt%Cr, 0.3–0.5 wt%Mo, 1.0 wt% Ni, 0.2 wt%Mn, or 0.12 wt%V. The reason for the enhancement of hardenabiblity is that B can retard the austenite to ferrite and pearlite transformation, thus enabling the martensite formation [3–6]. The effect of B on suppressing the ferrite formation is proposed to be due to non-equilibrium segregation of B at prior austenite grain boundaries (PAGBs) during cooling [3,6–22], which may reduce the grain boundary energy, and thus the efficiency of the PAGB to support heterogeneous nucleation of ferrite. Different from the equilibrium segregation [23] which is driven by the difference in free enthalpy of solute atoms in the matrix and at interfaces, the non-equilibrium segregation is associated with the formation of a large vacancy supersaturation and solute atom–vacancy complexes during cooling from high temperatures. Since grain boundaries (GBs) act as sinks for vacancies, a vacancy concentration gradient appears between GBs and the inner grain volume. Driven by the vacancy concentration gradient, solute atom–vacancy complexes diffuse towards GBs, leading to segregation of solute atoms at GBs. As the austenitization temperature and the cooling rate determine the vacancy concentration and its gradient, the magnitude of non-equilibrium segregation strongly depends on these two processing parameters [2,6,13,14].

Besides the above-mentioned processing conditions, alloying elements also influence the B segregation behavior at PAGBs and hence the hardenability of steels. For example, an addition of Nb [4] or Mo [2–4] to B-added low carbon steels can additionally enhance the hardenability of steels, whereas an addition of Cr has a smaller effect than Nb and Mo [5]. According to the continuous cooling transformation (CCT) curves reported in [3], the austenite to ferrite transformation is dramatically retarded by the addition of Mo. The reason behind this phenomenon was explained by the suppression of borocarbide $M_{23}(C, B)_6$ (a preferential site for ferrite nucleation) by Mo and Nb, rendering more B in solution during austenitization treatment and consequently more B at PAGBs upon cooling [4]. Another reason for this excellent synergistic effect of B and Mo on the hardenability of steels was proposed to be due to a drag effect of Mo on B by forming Mo–B–vacancy complexes [16]. However, a recent work by the present authors showed that the

* Corresponding authors. Fax: +49 211 6792333.
E-mail addresses: y.li@mpie.de (Y.J. Li), d.ponge@mpie.de (D. Ponge).

http://dx.doi.org/10.1016/j.ultramic.2015.03.009
0304-3991/

Table 1
Nominal chemical compositions (in wt% and at%) of Mo-added [24] and Cr-added Mo-free steels.

Elements		C	Si	Mn	Cr	Mo	Al	Nb	V	B
Mo-free	wt%	0.16	0.33	1.38	0.50	–	0.06	–	–	0.0025
	at%	0.71	0.65	1.39	0.53	–	0.12	–	–	0.0128
Mo-added	wt%	0.19	0.35	1.20	0.20	0.50	0.06	0.03	0.03	0.0024
	at%	0.88	0.69	1.21	0.21	0.29	0.12	0.02	0.03	0.0124

Gibbs interfacial excess value of B at a PAGB is four times higher than that of Mo [24]. This means that the formation of Mo–B–vacancy complexes may not be a major mechanism determining the B segregation. Recently, Han et al. reported that the synergistic effect of the combined addition of alloying elements with B on the hardenability of steel depends on the cooling rate [5]. For a cooling rate between 3 and 20 K/s an addition of 0.5 wt% Mo to the B-added steel provides a much higher hardenability than that of 0.5 wt% Cr does, whereas for the cooling rate ≥20 K/s the two alloying elements exhibit the same effect on the hardenability [5]. Such cooling rate-dependent effects of alloying elements on the hardenability may be associated with the cooling rate-dependent segregation behavior of B at PAGBs.

So far, segregation of B at PAGBs in martensitic steels has been studied by Particle Tracking Autoradiography (PTA) [3,6,15,20,22], Secondary Ion Mass Spectrometry (SIMS) [6,22,25,26] and Electron Energy Loss Spectroscopy (EELS) [21]. These characterization techniques are advantageous to large scale (up to several hundred micrometers) investigations, providing overviews of distributions of B at GBs and B-containing precipitates. However, it is

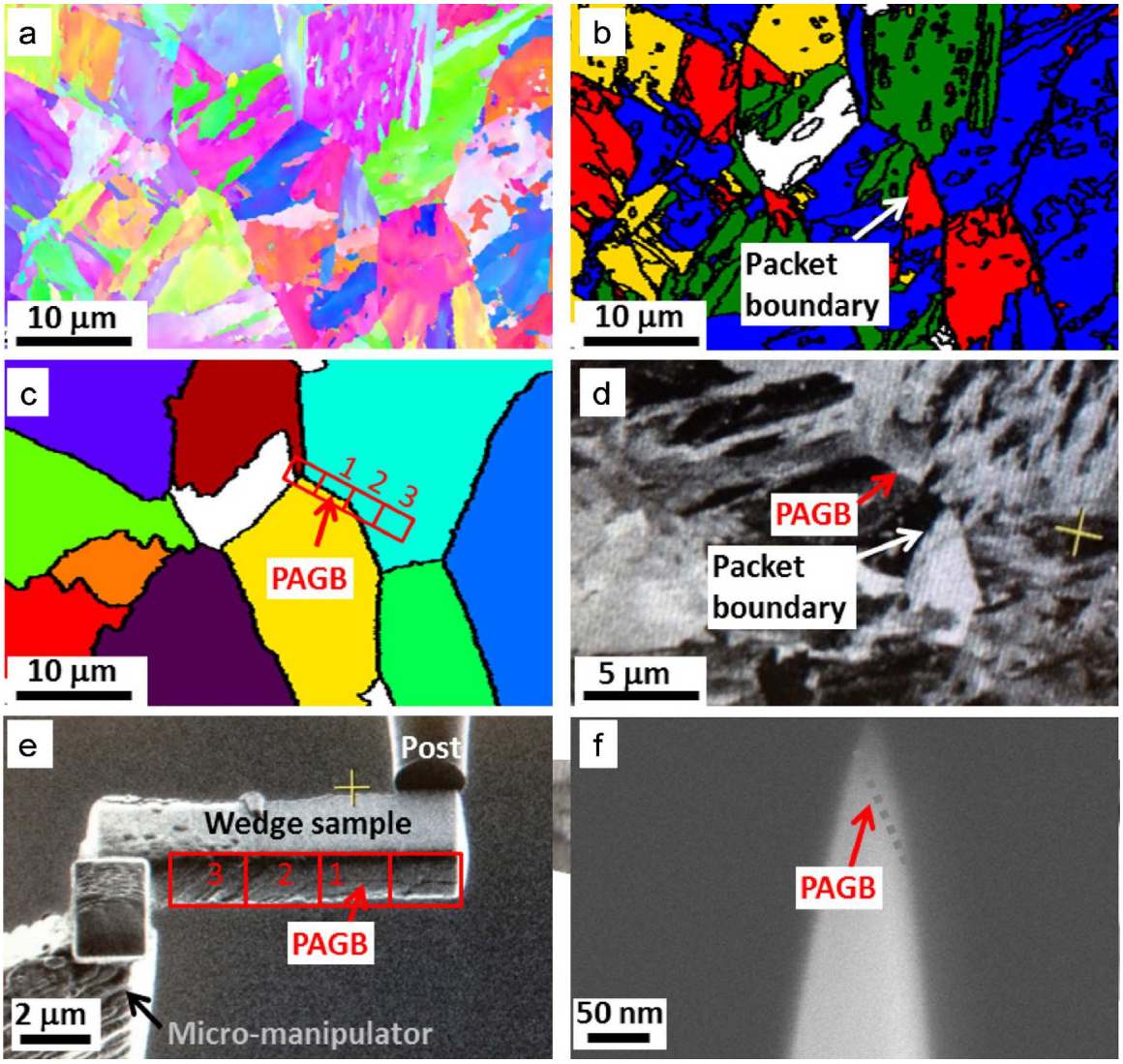

Fig. 1. Reconstruction of PAGBs and site-specific preparation of APT sample containing a PAGB. (a) Crystal orientation map measured using EBSD in SEM. (b) Reconstructed images displaying packet (identified by colors) and block boundaries (black lines within the packets). Unindexed regions are marked by white color. (c) Reconstructed austenite grains. Black lines are PAGBs. Red rectangles and the numbers mark the 3 analysis regions containing a PAGB (1), containing matrix at distances of 2 μm (2) and 5 μm (3) from the PAGB. (d) FIB image of correlative PAGBs as marked in (c) with the red arrow. The white arrows in (b) and (d) mark one correlative packet boundary. (e) FIB image showing alignment of the sample wedge on a post of a microtip array. Red rectangles and the numbers are correlative with those shown in (c). (f) A final APT tip containing the PAGB. (For interpretation of the references to color in this figure caption, the reader is referred to the web version of this paper.)

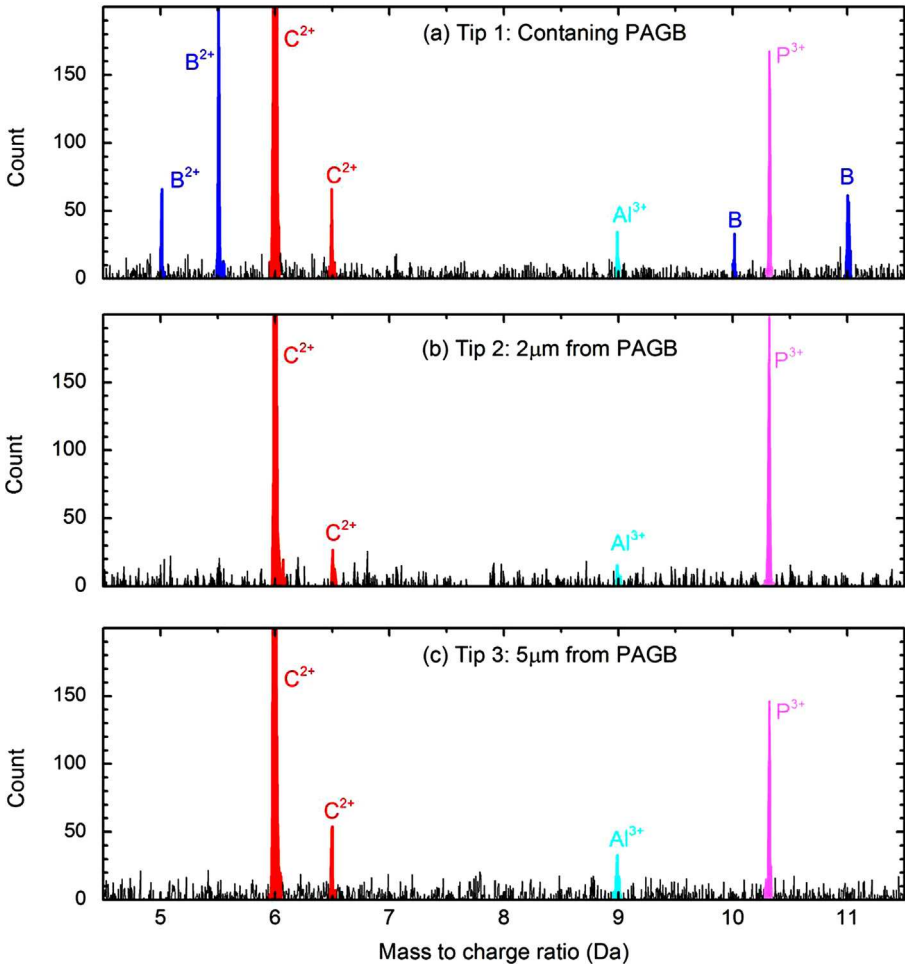

Fig. 2. Mass spectra of a quenched martensitic steel. (a) Tip 1 containing a PAGB shows B peaks (blue). (b) and (c) Tips located at distances of 2 μm and 5 μm away from the PAGB, respectively. Very little B peak is detected there. (For interpretation of the references to color in this figure caption, the reader is referred to the web version of this paper.)

challenging to obtain quantitative data using these techniques. Atom Probe Tomography (APT), as a complementary technique, yields precise information on solute distribution at GBs, in precipitates, and in the matrix at the atomic scale. Thus, APT is essential for fundamental understanding of grain boundary segregation and for optimizing the contents of B and other alloying elements to achieve optimal hardenability of low-carbon steels.

In the present work we apply APT to quantitatively investigate the distribution of B and other alloying elements (C, Cr, Mn and Si) at PAGBs and martensite–martensite boundaries, as well as in the martensite matrix of a quenched Cr-added Mo-free martensitic steel. For the present material a transformation of austenite to martensite occurred upon cooling. The quenched microstructure contains various boundaries, such as PAGBs and the newly formed packet and block boundaries as well as the martensite lath boundaries. For simplicity the newly formed boundaries during cooling are referred to as martensite–martensite (M–M) boundaries. The first step to prepare APT samples containing a PAGB is to distinguish PAGBs from the other types of boundaries. It is known that chemical etching can reveal PAGBs for tempered martensite [25], however, it does not work for a quenched martensite. In this work, prior austenite grains (PAGs) were reconstructed from electron backscatter diffraction (EBSD) orientation maps. Subsequently, FIB milling was applied for site-specific preparation of APT samples containing PAGBs. In order to elucidate the effect of Mo on B segregation at PAGBs, the results were compared with our recent work conducted on a Mo-added steels [24]. Additionally, the underlying mechanisms of segregation of B and C are discussed.

2. Experimental

2.1. Materials and processing

The chemical compositions of the Cr-added Mo-free and Mo-added [24] low-carbon steels are listed in Table 1. It should be noted that Nb and V, which have been proposed to have a strong synergistic effect together with B on the steel's hardenability [5], are present in the Mo-added steel [24] but absent in the Mo-free steel. In both alloy variants Al was added to protect B from B nitriding.

The steel was austenitized at 1203 K for 30 min followed by water quenching. The cooling rate at the APT sampling location was approximately 30 K/s within the first 20 s of quenching from 1203 K. It is worth noting that the two main parameters influencing the segregation behavior of B, i.e., the austenitization temperature and the cooling rate, are the same for the Cr-added Mo-free steel as for the Mo-added steel.

2.2. Site-specific APT sample preparation from prior austenite grain boundaries

A software, developed by CEA-Grenoble, Laboratory of

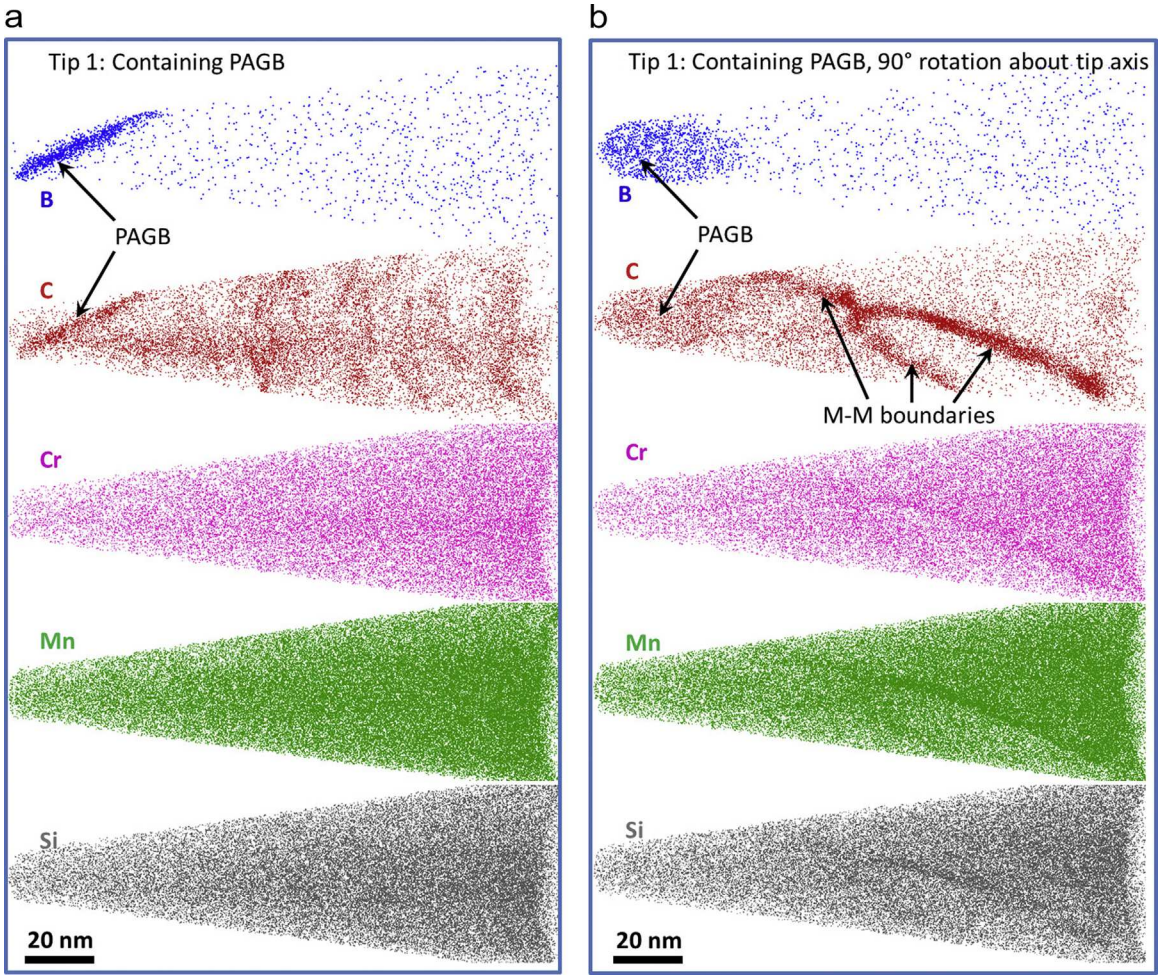

Fig. 3. 3-D atom maps of the as-quenched martensitic steel for tip 1 containing a PAGB. (a) Views perpendicular to the normal of PAGB plane showing segregation of B and C and no segregation of Cr, Mn, and Si at the PAGB. (b) Views along the normal of PAGB plane showing significant segregation of C, slight segregation of Cr, Mn, and Si, and no segregation of B at M–M boundaries.

Innovation for New Energy Technologies and Nanomaterials, France, was applied for reconstructing the PAGBs from Electron Back Scatter Diffraction (EBSD) data according to the orientation relationship (Kurdjumov-Sachs) between the martensite variants and their parent austenite grain (see details in [27]).The EBSD measurement was performed using a step size of 80 nm. Fig. 1a shows the EBSD orientation map of the as-quenched steel containing various unidentified boundaries. The different colors in Fig. 1b are identified as reconstructed packets. The black lines inside the packets are block boundaries. The martensite lath boundaries are not resolvable due to the large step size. Fig. 1c shows the reconstructed PAGBs. The PAGB to be investigated by APT is marked by red arrows. The distribution of the alloying elements was analyzed for the three selected regions. One of them contains a PAGB (tip 1). The other two regions are located in the martensite matrix at distances of 2 μm (tip 2) and 5 μm (tip 3) away from the PAGB (see the corresponding red rectangles in Fig. 1c). Fig. 1d shows the focused ion beam (FIB) induced secondary electron image. Referring to the reconstructed PAGBs in Fig. 1c the correlative PAGB (marked with the red arrow in Fig. 1d) can be positioned when preparing APT samples containing PAGBs. Clearly, the correlative boundary marked by the white arrows in Fig. 1b and d is not a PAGB, but a packet boundary, which does not appear in Fig. 1c as a non-PAGB.

Site-specific preparation of APT samples containing PAGBs were performed using a dual beam FIB (FEI Helios NanoLab 600TM) according to the procedures described in [28]. The boundary marked by the red arrow (Fig. 1d) was lifted out as shown in Fig. 1e. Fig. 1f shows the final APT tip containing the PAGB.

2.3. APT measurement

A local electrode atom probe (LEAP) (LEAP 3000X HR™, Cameca Instruments) was employed to analyze the element distributions. The measurements were performed in voltage mode with a pulse fraction of 15% at 70 K and at a detection rate of 0.005 atoms per pulse.

3. Results

Fig. 2 shows the mass spectra of the Cr-added Mo-free steel analyzed at three different locations. The blue peaks in Fig. 2a at mass to charge ratios of 5 Da, 5.5 Da, 10 Da, and 11 Da are assigned as B. Very little B peak is observed in the tips not containing PAGBs (Fig. 2b and c). This means that very few B atoms are detected in the martensite matrix.

The atom maps of the sample containing a PAGB (tip 1) are shown in Fig. 3. Fig. 3a and b are the views perpendicular and parallel to the normal of the PAGB plane, respectively. The M–M boundaries close to the PAGB are also contained in the probed volume. The planes of the M–M boundaries are perpendicular to

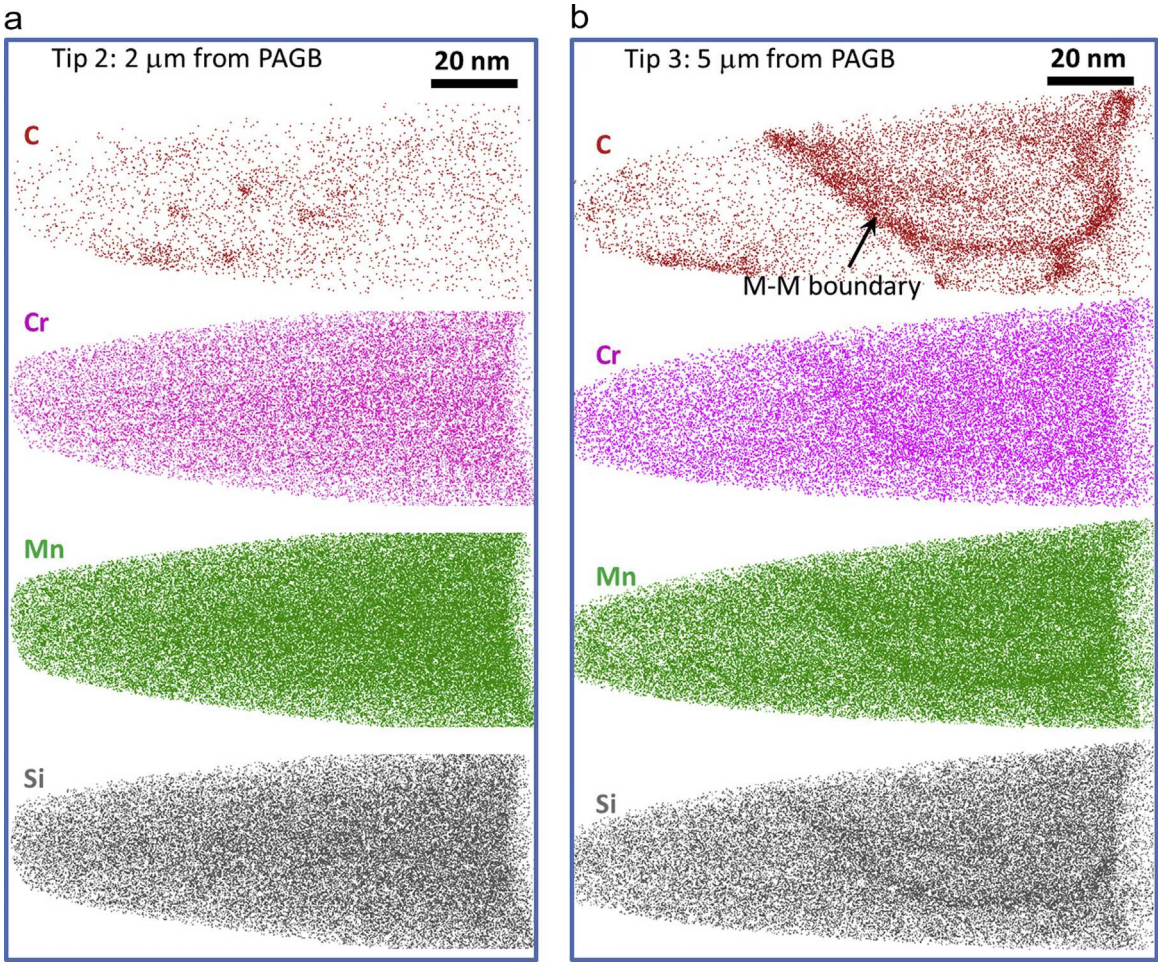

Fig. 4. 3-D atom maps of the as-quenched martensitic steel for (a) tip 2 and (b) tip 3 cut from locations of 2 μm and 5 μm away from the PAGB, respectively. B is neither detected in the matrix nor at the M–M boundary.

the PAGB plane. A rotation by 90° about the tip axis in Fig. 3a clearly reveals the M–M boundaries, as indicated by the arrows in Fig. 3b. It is seen that B is only segregated to the PAGB, whereas C is segregate to both PAGB and M–M boundaries. Unlike Mo [24], Cr, Mn, and Si atoms are not segregated at the PAGB (Fig. 3a), but slightly segregated at the M–M boundaries (Fig. 3b).

Fig. 4a and b displays the atom maps obtained from tip 2 and tip 3 taken from the martensite matrix at distances of 2 μm and 5 μm away from the PAGB, respectively. No B is observed in the probed volumes. While tip 2 does not contain any interface, C is not homogeneously distributed in the martensite matrix, but C clusters can be observed. Cr, Mn, and Si are homogeneously distributed (Fig. 4a). In tip 3 a M–M boundary with strong C segregation and slight segregation of Cr, Mn, and Si is detected. These results suggest that B is neither distributed in the martensite matrix nor segregated to the M–M boundary.

The quantitative analyses of the elements at PAGBs and M–M boundaries are performed for the selected regions of interest (ROIs) as shown in Fig. 5a and b. The 1D concentration profiles are plotted along the arrow directions. Fig. 5c shows that the C concentration at the PAGB is about six times higher than its nominal value of 0.71 at%. Similar to the result on the Mo-added steel [24] the concentration of B (1.68 at%) at the PAGB in the Cr-added Mo-free steel is also two orders of magnitude higher than its nominal value of 0.013 at%. For Cr, Mn, and Si no concentration peaks are observed here at the PAGB. At the M–M boundary (see Fig. 5b and d) only a concentration peak for C is observed. In agreement with the result shown in Fig. 3b no concentration peak for B is observed at the M–M boundary. While a weak contrast of Cr, Mn, and Si is visualized at the M–M boundaries (Figs. 3b and 4b), no peak in their concentration profiles (Fig. 5b) is observed. This may be attributed to a locally high density of Fe atoms at the same boundary, enhancing the total number of atoms there, so that the obtained concentration (ratio of the number of these substitutional atoms to the total number of all atoms) profiles remain as low as that in the matrix (Fig. 5d). Comparing Fig. 5c with Fig. 5d reveals that the concentration profiles of Cr, Mn, and Si across the M–M boundary exhibit the same concentration values as those across the PAGB. In both cases the measured concentrations are approximately equal to their corresponding nominal values (see Table 1), indicating that these elements are mostly homogeneously distributed throughout the volume.

For an accurate assessment of the degree of segregation of solutes at the PAGB the Gibbs interfacial excess value Γ_X of solute X (atoms per grain boundary area) can be derived from the concentration profiles shown in Fig. 5c. The details of the method are described in [29]. The Gibbs interfacial excess Γ_X of a solute is a more suitable quantity than the concentration for quantifying solute segregation in different materials, as it is less sensitive to reconstruction artifacts and the probing direction. The concentration could be underestimated to a certain extent due to the local magnification effect [30]. The numbers of solutes N_C and N_B on the PAGB plane with an area of 305 nm^2 are marked in Fig. 6a and b by the red and blue double arrows, respectively. For comparison the N_C and N_B values on the same area of PAGB for the Mo-added steel are also plotted (small open squares). In the same

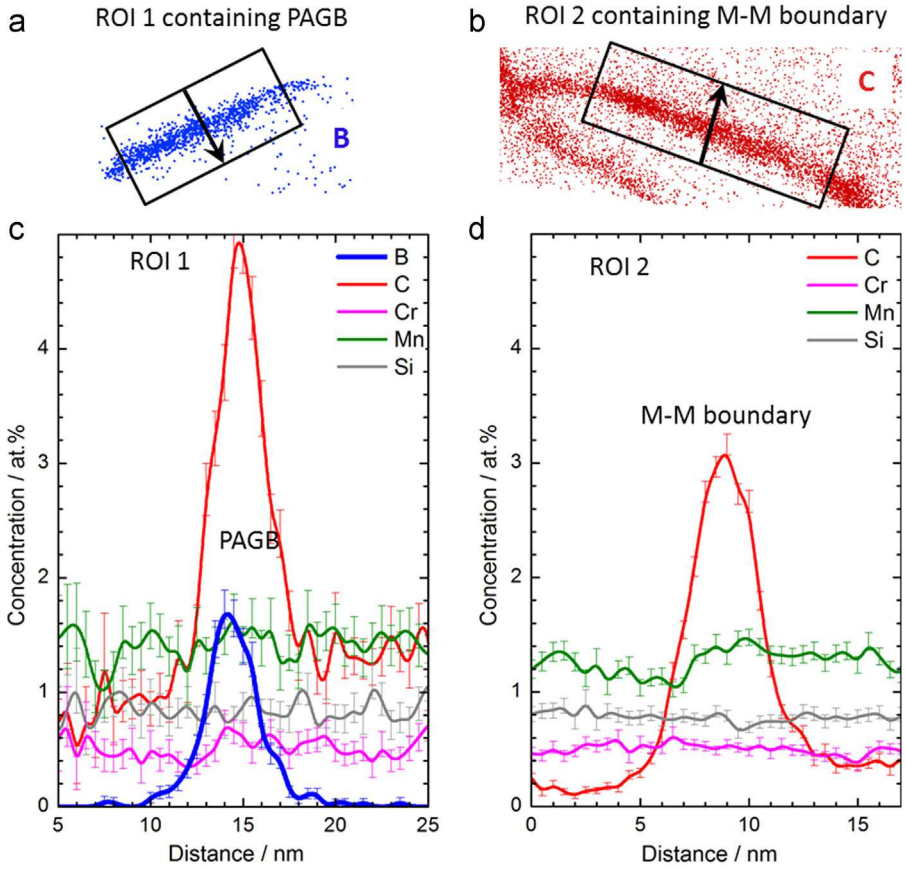

Fig. 5. (a) ROI 1 and (b) ROI 2 are selected for concentration analysis across the PAGB and the M–M boundary, respectively. (c) and (d) are the corresponding 1-D concentration profiles within the ROIs along the directions marked by the black arrows in (a) and (b). ROI: region of interest.

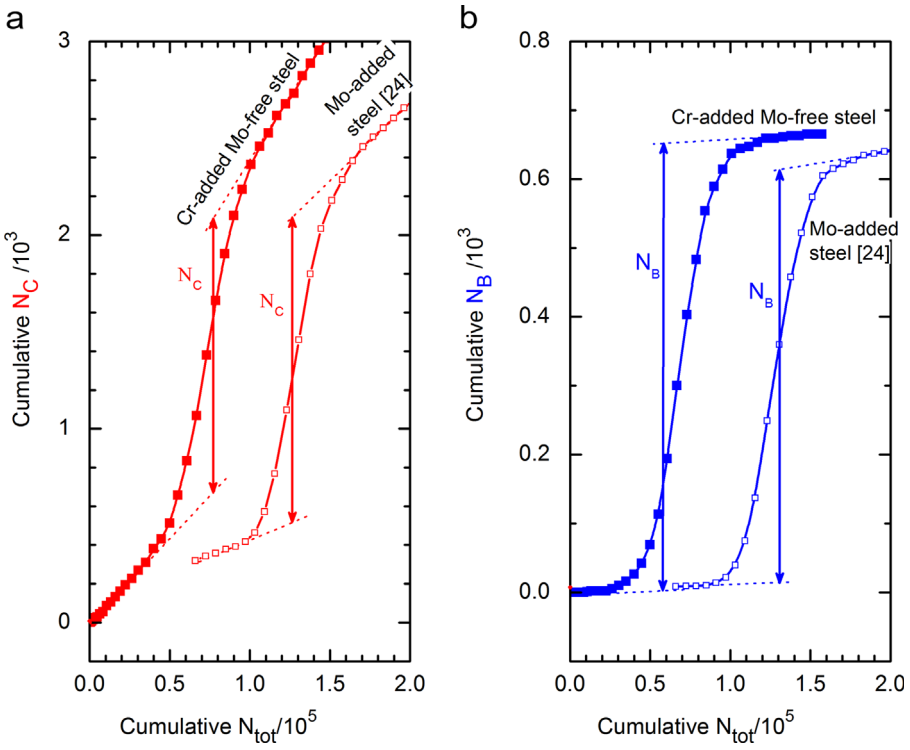

Fig. 6. Determination of grain boundary excess number of C and B from the APT analyses of ROI 1 shown in Fig. 5 according to the method described in [29]. The data from [24] for the Mo-added steel are displayed for comparison. (For interpretation of the references to color in this figure, the reader is referred to the web version of this paper.)

given boundary area there are more carbon atoms for the Mo-added steel than that for the Cr-added Mo-free steel (Fig. 6a). Both steels show similar N_B values (Fig. 6b), which correspond to the B excess values Γ_B of 5.27 atoms nm^{-2} and 5.87 atoms nm^{-2} for Mo-added and Cr-added Mo-free steels, respectively.

4. Discussion

It is generally accepted that B segregation to PAGBs upon cooling is controlled by a non-equilibrium mechanism [3,6,10–16,19–22], i.e., segregation occurs by formation and diffusion of vacancy–solute complexes towards grain boundaries. The present work shows that while M–M boundaries, like PAGBs, also act as sinks for vacancies, B is segregated to the PAGB, but not to the M–M boundaries. The absence of B segregation at the M–M boundaries indicates that all B atoms which originally dissolved in the matrix are segregated to PAGBs and such segregation occurs before the austenite to martensite transformation takes place. Thus, B segregation at PAGBs should occur during cooling in the high temperature range (at least above the starting temperature of martensite formation, i.e., 673 K for the present steel). It is known that non-equilibrium segregation occurs at high temperatures and its extent increases with temperature due to an increase in the available vacancy concentration. In contrast, the equilibrium segregation becomes negligible with temperature, as the solutes tend to be homogeneously distributed with increasing temperature. Therefore, the observed segregation of B at the PAGB is probably of non-equilibrium type. Due to the absence of a measured value for the binding energy between B and PAGBs in the low carbon steel the contribution to the observed segregation from the equilibrium type is hard to estimate according to the McLean segregation theory [23]. Our recent work on the Mo-added steel reveals that only the solutes (B, Mo, P, and Nb) which have high binding energies with vacancies [31] were observed to segregate at PAGBs [24], whereas solutes such as Cr and Mn which have low binding energies with vacancies [31,32] are not segregated there. These results are confirmed by the present observations on the Cr-added Mo-free steel. The correlation between the segregation behaviors of solutes and their binding energies with vacancies strongly suggests a vacancy-associated segregation type, i.e., a non-equilibrium mechanism controlling the B segregation at PAGBs. It should be mentioned that although Si has a significant binding energy of 0.35 with vacancies [31], the recombination of Si with vacancies is strongly limited by its low diffusivity in austenite [31]. Therefore, the segregation of Si at the PAGBs by a non-equilibrium mechanism is not observed here (Fig. 3a).

C is observed to be segregated both at PAGBs and at the M–M boundaries. The same results were also reported on the Mo-added steel [24]. During cooling after martensite formation, the extremely supersaturated martensite with all remaining solutes such as C, Si, Mn, and Cr enhances the total system free energy, and thus the reduction of the energy acts as a driving force for solute segregation to M–M boundaries. The fast diffusion of C and the high density of defects (short diffusion length) in the martensite kinetically enable such segregation of C at M–M boundaries during cooling, whereas segregation of Si, Mn, and Cr at the M–M boundaries is slight and kinetically limited due to the low diffusivities of these elements [24,33–36]. As shown in Figs. 3 and 4b as well as in the literature [24,37] segregation of C at the M–M boundaries is generally observed in as-quenched martensitic steels. The mechanism controlling the segregation at the M–M boundaries is unambiguously of equilibrium type.

Segregation of C at PAGBs may also occur after the formation of martensite through an interstitial diffusion mechanism, i.e., the equilibrium segregation mechanism [38,39]. Non-equilibrium segregation of C at PABGs may be unlikely. As given by Williams et al. [11] one of the conditions for non-equilibrium solute segregation to occur is that the solute does not diffuse rapidly enough to eliminate segregation. Noting that non-equilibrium segregation occurs at high temperatures where no thermodynamic driving force exists for the equilibrium segregation, even if C atoms are driven by the vacancy concentration gradient towards PAGBs through forming C–vacancy complexes, the back diffusion of C at high temperature through the fast interstitial diffusion mechanism can considerably reduce the amount of segregation. Thus, the observed enrichment of C at the PAGB is mainly attributed to a equilibrium segregation mechanism.

Our recent results on the Mo-added steel suggest that the formation of B–Mo-complexes may not be the major mechanism of B segregation at PAGBs. The formation and diffusion of B–vacancy complexes is instead assumed to be the controlling mechanism [24]. In the present Mo-free steel we found virtually the same segregation behavior of B as that in the Mo-added steel. In both steels no B is detected in the martensite matrix, and similar B excess values at PAGBs are obtained. The results on the Mo-free steel confirm again that, without Mo, B atoms which were originally dissolved in the matrix can be all segregated to PAGBs upon cooling from 1203 K at a cooling rate of 30 K/s. In the Mo-free steel there are more Cr atoms than that in the Mo-added steel. Since no Cr segregation is observed at the PAGB, the extra Cr in the Mo-free steel should not account for the B segregation at PAGBs. It is reported that a low carbon B-added steel containing 0.5 wt% Mo exhibits the same hardenability as that of a 0.5 wt% Cr-containing steel [5] for cooling rates $\geq$20 K/s. This result may be explained by the same segregation behavior of B in both steels at the cooling rate of $\geq$30 K/s.

5. Conclusions

The site-specific preparation of APT tips containing a prior austenite grain boundary was applied to study the segregation behavior of B and other alloying elements such as C, Mn and Si in a quenched Cr-added Mo-free martensitic steel. The PAGBs were reconstructed from EBSD data according to the orientation relationship between the martensite variants and their parent austenite grain, and thus were distinguished from the M–M boundaries. Segregation of B at the PAGB and its absence at the M–M boundaries indicate a non-equilibrium mechanism controlling the B segregation behavior. We propose that C segregation, both at the PAGB and the M–M boundaries, occurs by interstitial diffusion, i.e., an equilibrium segregation mechanism. Probably low binding energies of Cr and Mn with vacancies inhibit non-equilibrium segregation of these elements to PAGBs, while low diffusivities limit significant equilibrium segregation of these element to M–M boundaries. The observation of the same segregation behavior of B in the Mo-free steel as that in the Mo-added steel confirms that no Mo drag effect on the B segregation exists under the current heat treatment conditions.

Acknowledgments

The research leading to these results has received funding from the European Union's Research Fund for Coal and Steel (RFCS) research programme under Grant agreement no. [RFCS-CT-2012-00018]. The authors thank Mr. M. Green from Tata Steel Research and Development for providing the steel samples. We also thank Dr. H. Zhang from Max-Planck Institut für Eisenforschung for

valuable discussions. Dr. I. Gutierrez, Mr. M. Green, Dr. W. Xu, and Dr. I. Tolleneer are gratefully acknowledged for their scientific and technical supports within the RFCS-project.

References

[1] M.A. Grossmann, Hardenability calculated from chemical composition, Trans. Metall. Soc. AIME 150 (1942) 227–259.
[2] M. Ueno, K. Itoh, The optimum condition to obtain the maximum hardenability effect of boron, Tetsu-to-Hagané 74 (1988) 910–917.
[3] H. Asahi, Effects of Mo addition and austenitizing temperature on hardenability of low alloy B-added steels, ISIJ Int. 42 (2002) 1150–1155.
[4] T. Hara, H. Asahi, R. Uemori, H. Tamehiro, Role of combined addition of niobium and boron and of molybdenum and boron on hardnenability in low carbon steels, ISIJ Int. 44 (2004) 1431–1440.
[5] F. Han, B. Hwang, D.W. Suh, Z. Wang, D.L. Lee, S.J. Kim, Effect of molybdenum and chromium on hardenability of low-carbon boron-added steels, Met. Mater. 14 (2008) 667–672.
[6] D.J. Mun, E.J. Shin, K.C. Cho, J.S. Lee, Y.M. Koo, Cooling rate dependence of boron distribution in low carbon steel, Metall. Mater. Trans. A 43 (2012) 1639–1648.
[7] K.T. Aust, S.J. Armijo, E.F. Koch, J.H. Westbrook, Intergranular corrosion and electron microscopic studies of austenitic stainless steels, Trans. Am. Soc. Met. 60 (1967) 360–372.
[8] T.R. Anthony, R.E. Hanneman, Non-equilibrium segregation of impurities in quenched dilute alloys, Scr. Metall. 2 (1968) 611–614.
[9] K.T. Aust, R.E. Hanneman, P. Niessen, J.H. Westbrook, Solute induced hardening near grain boundaries in zone refined metals, Acta Metall. 16 (1968) 291–302.
[10] J.D. Garnish, J.D.H. Hughes, Quantitative analysis of boron in solids by autoradiography, J. Mater. Sci. 7 (1972) 7–13.
[11] T.M. Williams, A.M. Stoneham, D.R. Harries, The segregation of boron to grain boundaries in solution-treated type 316 austenitic stainless steel, Met. Sci. 10 (1976) 14–19.
[12] L. Karlsson, H.O. Andrén, H. Nordén, Grain boundary segregation in an austenitic stainless steel containing boron - an atom-probe study, Scr. Metall. 16 (1982) 297–302.
[13] L. Karlsson, H. Nordén, H. Odelius, Overview no. 63 non-equilibrium grain boundary segregation of boron in austenitic stainless steel. I. Large scale segregation behaviour, Acta Metall. 36 (1988) 1–12.
[14] X.L. He, Y.Y. Chu, J.J. Jonas, Grain boundary segregation of boron during continuous cooling, Acta Metall. 37 (1989) 147–161.
[15] X.L. He, M. Djahazi, J.J. Jonas, J. Jackman, The non-equilibrium segregation of boron during the recrystallization of Nb-treated HSLA steels, Acta Metall. 39 (1991) 2295–2308.
[16] S. Dumbill, R.M. Boothby, T.M. Williams, Grain boundary segregation in Nimonic PE16, Mater. Sci. Technol. 7 (1991) 385–390.
[17] K.A. Taylor, Grain-boundary segregation and precipitation of boron in 0.2 percent carbon steels, Metall. Trans. A 23 (1992) 107–119.
[18] T. Xu, Non-equilibrium segregation to grain boundaries, Scr. Metall. 37 (1997) 1643–1650.
[19] T. Sourmail, T. Okuda, J.E. Taylor, Formation of chromium borides in quenched modified 310 austenitic stainless steel, Scr. Mater. 50 (2004) 1271–1276.
[20] B. Hwang, D.W. Suh, S.J. Kim, Austenitizing temperature and hardenability of low-carbon boron steels, Scr. Mater. 64 (2011) 1118–1120.
[21] G. Shigesato, T. Fujishiro, T. Hara, Boron segregation to austenite grain boundary in low alloy steel measured by aberration corrected STEM EELS, Mater. Sci. Eng. A 556 (2012) 358–365.
[22] S. Kim, Y. Kang, C. Lee, Variation in microstructures and mechanical properties in the coarse-grained heat-affected zone of low-alloy steel with boron content, Mater. Sci. Eng. A 559 (2013) 178–186.
[23] D. McLean, Grain Boundaries in Metals, Oxford University Press, London, 1957.
[24] Y.J. Li, D. Pong, P. Choi, D. Raabe, Segregation of boron at prior austenite grain boundaries in a quenched martensitic steel studied by atom probe tomography, Scr. Mater. 96 (2015) 13–16.
[25] J.B. Seol, N.S. Lim, B.H. Lee, L. Renaud, C.G. Park, Atom probe tomography and nano secondary ion mass spectroscopy investigation of the segregation of boron at austenite grain boundaries in 0.5 wt% carbon steels, Met. Mater. Int. 17 (2011) 413–416.
[26] F. Liu, D.H.R. Fors, A. Golpayegani, H.O. Andrén, G. Wahnström, Effect of boron on carbide coarsening at 873 K (600°C) in 9 to 12 pct chromium steels, Metall. Mater. Trans. 43 (2012) 4053–4062.
[27] C. Cayron, ARPGE: a computer program to automatically reconstruct the parent grains from electron backscatter diffraction data, J. Appl. Cryst. 40 (2007) 1183–1188.
[28] K. Thompson, D. Lawrence, D.J. Larson, J.D. Olson, T.F. Kelly, B. Gorman, In situ site-specific specimen preparation for atom probe tomography, Ultramicroscopy 107 (2007) 131–139.
[29] B.W. Krakauer, D.N. Seidman, Absolute atomic-scale measurements of the Gibbsian interfacial excess of solute at internal interfaces, Phys. Rev. B 48 (1993) 6724–6729.
[30] M.K. Miller, M.G. Hetherington, Local magnification effects in the atom probe, Surf. Sci. 246 (1991) 442–449.
[31] R.G. Faulkner, Impurity diffusion constants and vacancy–impurity binding energies in solids, Mater. Sci. Technol. 1 (1985) 442–447.
[32] T.P.C. Klaver, D.J. Hepburn, G.J. Ackland, Phys. Rev. B 85 (2012) 174111.
[33] C.G. Lee, Y. Iijima, T. Hiratani, K. Hirano, Diffusion of chromium in α-iron, Mater. Trans. JIM 31 (1990) 255–261.
[34] Y.J. Li, P. Choi, S. Goto, C. Borchers, D. Raabe, R. Kirchheim, Evolution of strength and microstructure during annealing of heavily cold-drawn 6.3 GPa hypereutectoid pearlitic steel wire, Acta Mater. 60 (2012) 4005–4016.
[35] Y.J. Li, P. Choi, S. Goto, C. Borchers, D. Raabe, R. Kirchheim, Atomic scale investigation of redistribution of alloying elements in pearlitic steel wires upon cold-drawing and annealing, Ultramicroscopy 132 (2013) 233–238.
[36] Y.J. Li, A. Kostka, P. Choi, S. Goto, D. Ponge, R. Kirchheim, D. Raabe, Mechanisms of subgrain coarsening and its effect on the mechanical properties of carbon-supersaturated nanocrystalline hypereutectoid steel, Acta Mater. 84 (2015) 110–123.
[37] L. Yuan, D. Ponge, J. Wittig, P. Choi, J.A. Jiménez, D. Raabe, Nanoscale austenite reversion through partitioning, segregation and kinetic freezing: Example of a ductile 2 GPa Fe Cr C steel, Acta Mater. 60 (2012) 2790–2804.
[38] Y.J. Li, D. Raabe, M. Herbig, P. Choi, S. Goto, A. Kostka, H. Yarita, C. Borchers, R. Kirchheim, Segregation stabilizes nanocrystalline bulk steel with near theoretical strength, Phys. Rev. Lett. 113 (2014) 1061043.
[39] M. Herbig, D. Raabe, Y.J. Li, P. Choi, S. Zaefferer, S. Goto, Atomic-scale quantification of grain boundary segregation in nanocrystalline material, Phys. Rev. Lett. 112 (2014) 126103.